National Centre for Energy and Environment,
Energy Commission of Nigeria, University of Benin:
ISSN 2504-9593
DOI: 10.5281/zenodo.21874498
https://ijree.com/index.php/publications/article/view/92
Int. J. Renew. Energ & Environ Vol.4 (2), pp 598-616(2026)

# FLOOD SUSCEPTIBILITY MAPPING IN SOUTHERN PLATEAU STATE, NIGERIA USING FREQUENCY RATIO MODEL AND GEOSPATIAL TECHNIQUES

**[1]Songtak, N., [2]Jang, P.D., [3]Ramnap, N.V., [4]Nimlang, H.N., [5]Ogbole, A.S., [6]Zitta, Y.L.**
[1,2,3,4] National Space Research and Development Agency, Abuja; [5]Department of Geography, Plateau State University, Bokkos; and [6] Telpon Environment Limited
[4]Corresponding Author: nanloknimlang@yahoo.com

***Abstract***
*Flooding is a significant natural hazard in Sub-Saharan Africa, exacerbated by climate variability, rapid urbanisation, and inadequate drainage systems. This study aims to develop and validate a high-resolution (30 m) flood susceptibility map for Southern Plateau State, Nigeria, using the Frequency Ratio (FR) model and multi-source geospatial datasets. Specifically, the study aims to develop a flood inventory from Sentinel-1 SAR imagery and ancillary records, evaluate the influence of ten flood-conditioning factors, generate a Flood Susceptibility Index (FSI), assess model performance using independent validation and spatial-block cross-validation, and provide a decision-support tool for flood risk management and land-use planning. A flood inventory derived from Sentinel-1 SAR flood extents (2021–2022) and ancillary records was divided into training (70%) and validation (30%) datasets. Ten flood-conditioning factors, including elevation, Topographic Wetness Index, rainfall, land use/land cover, NDVI, lineament density, soil type, geology, and distances to rivers and roads were incorporated into the model. The FR model demonstrated excellent predictive performance (AUC = 0.933; 95% CI: 0.882–0.983), with spatial-block cross-validation confirming its robustness (mean AUC = 0.933 ± 0.034). Rainfall, drainage density, built-up areas, elevation, and lineament density were the most influential flood drivers, while High and Very High susceptibility zones occupied 19.13% of the study area. The resulting susceptibility map provides a reproducible framework and practical decision-support tool for flood risk management, land-use planning, and climate adaptation in data-scarce regions. State and local planning authorities should integrate the flood susceptibility map into development control, environmental impact assessment, and urban expansion planning to reduce future flood exposure.*
***Keywords: Geographic Information Systems, Frequency Ratio, Flood Susceptibility Index, Frequency Ratio Model, Model Performance, Flood-Conditioning Factors, Cross Validation***

## 1. INTRODUCTION

Flooding is the most widespread natural hazard worldwide, affecting more people annually than any other weather-related disaster. Globally, over 2.5 billion people were affected by floods between 2000 and 2023, resulting in economic losses of about $1 trillion and roughly 40% of disaster-related deaths (UNDRR, 2020; IPCC, 2021; Shamsudduha, 2025). Increasing flood frequency and severity are driven by climate change, rapid urbanization, land-use transformation, and ecosystem degradation, with flood exposure projected to rise substantially by (Winsemius *et al*., 2016; Hirabayashi *et al*., 2021; Tellman *et al*., 2021; Rentschler *et al*., 2022). As a result, the Sendai Framework and the Sustainable Development Goals have made the production of accurate flood susceptibility maps a global priority for disaster risk reduction and sustainable land-use planning (UNDRR, 2015; Aitsi-Selmi *et al*., 2016). Advancements in Geographic Information Systems (GIS), remote sensing, and cloud computing have greatly enhanced flood susceptibility modelling by enabling the integration of topographic, hydrological, climatic, geological, and land-cover datasets at regional scales (Gorelick *et al*., 2017; Tien

Bui *et al*., 2019; Arabameri *et al*., 2020; Chen *et al*., 2023). Among statistical approaches, the Frequency Ratio (FR) model remains widely adopted due to its simplicity, transparency, and accurate predictive performance, particularly in data-scarce regions (Saha *et al*., 2021; Costache *et al*., 2022; Chen *et al*., 2023; Razavi-Termeh *et al*., 2023). Recent studies emphasize that integrating high-quality flood inventories with rigorous validation procedures, including independent datasets and spatial-block cross-validation, substantially improves model reliability and reduces spatial overfitting (Roberts *et al*., 2017; Nardi *et al*., 2019; Dottori *et al*., 2021; Demissie et al., 2024).

Flooding poses a major challenge across Sub-Saharan Africa due to rapid population growth, unplanned urbanization, limited institutional capacity, and high climate variability (Serdeczny *et al*., 2017; Shafik, 2025). Nigeria has experienced particularly severe flood disasters, with the 2012 and 2022 events affecting more than seven million people and causing economic losses exceeding US$10 billion (UNDRR, 2020; NEMA, 2022). However, flood susceptibility mapping in Nigeria remains fragmented and is often constrained by coarse-resolution datasets, limited flood inventories, inadequate validation, and insufficient consideration of geological controls (Ouma & Tateishi, 2014; Okoli *et al*., 2026).

Southern Plateau State, located along the southern margin of the Benue Trough, is highly vulnerable to flash flooding due to the intense seasonal rainfall, rugged terrain, rapid urban expansion, and the influence of complex geological formations on drainage patterns (Fashae *et al*., 2014; Epsar Philip Kopteer *et al*., 2024). Recent flood events have caused substantial damage to infrastructure, agricultural land, and livelihoods (NEMA, 2022). Despite this vulnerability, no comprehensive, rigorously validated flood susceptibility assessment has been conducted for the region. Previous studies have generally relied on coarse Digital Elevation Models (DEMs), single-source flood inventories, and conventional validation methods (Puno et al., 2022; Timité et al., 2022). In contrast, the contribution of geological lineament density to flood occurrence has received little attention (Okoli *et al*., 2026) .

Although previous studies have investigated flood hazards in parts of Nigeria and other comparable environments (Puno et al., 2022; Epsar Philip Kopteer et al., 2024b; Montien Tique et al., 2026), Southern Plateau State has not been the subject of a comprehensive and rigorously validated high-resolution flood susceptibility assessment. Furthermore, existing studies often rely on limited flood inventories, coarse-resolution datasets, simplified validation procedures, or fail to account adequately for the combined influence of hydrological, topographic, geological, and land-use factors. These scientific and methodological limitations highlight the need for a robust, high-resolution, and rigorously validated flood susceptibility assessment for Southern Plateau State. The study combines Sentinel-1 SAR-derived flood extents from the 2021 and 2022 flood events with a rigorously compiled multi-source flood inventory, ten flood-conditioning factors, including geological lineament density, and robust validation through independent testing and spatial-block cross-validation. This approach provides a systematic assessment of the relative influence of hydrogeomorphic, climatic, geological, and anthropogenic factors on flood occurrence within the southern Benue Trough.

The study aims to develop and validate a high-resolution flood susceptibility map for Southern Plateau State, Nigeria, using an integrated Frequency Ratio modelling framework and multi-source geospatial datasets. Specifically, it seeks to (i) develop a validated flood inventory from Sentinel-1 SAR imagery and ancillary records, (ii) derive and analyse ten flood-conditioning factors at 30 m resolution, (iii) generate and classify a Flood Susceptibility Index using the Frequency Ratio model, (iv) evaluate model performance using independent validation, confusion matrix metrics, and spatial-block cross-validation, (v) determine the relative importance of flood-conditioning factors, and (vi) provide an evidence-based decision-support tool for flood risk management, land-use planning, and climate adaptation in Southern zone of Plateau State.

This study makes three principal contributions. First, it presents the first regional application integrating Sentinel-1 SAR-derived flood extents, a multi-source flood inventory, and spatial-block cross-validation within an FR modelling framework for the Southern zone of Plateau State. Second, it provides the first systematic evaluation of ten flood-conditioning factors, uniquely incorporating geological lineament density, to quantify their relative contributions to flood susceptibility in the southern Benue Trough. Third, it delivers a validated 30 m flood susceptibility map that serves as a practical decision-support tool for flood risk management while providing a reproducible methodological framework for flood susceptibility assessment in other data-scarce regions of Sub-Saharan Africa.

## 2. MATERIALS AND METHODS

### 2.1 Study Area

The study area (see Figure 1) is located in the Southern zone of Plateau State, Nigeria, along the southern margin of the Benue Trough, spanning Longitude 8°30′E to 9°30′E and Latitude 8°N to 9°N. The area experiences a tropical savanna climate with distinct wet (June–September) and dry seasons. Mean annual rainfall ranges from 1,500 to 1,800 mm, with intense, high-magnitude events during the monsoon period that frequently trigger flash floods. The Shemankar River, a tributary of the Gongola River (Ogbole *et al.*, 2026), drains the area with a dendritic-to-subdendritic drainage pattern and high drainage density in steeper terrain. Bedrock geology comprises Jurassic Younger Granites and Precambrian Basement Complex rocks, overlain by lateritic deposits and transected by major fault lineaments that influence drainage patterns. Soils are predominantly Ferrasols and Lixisols, shallow, well-drained, highly weathered, with high gravel content and susceptibility to erosion. Land use, particularly in the Wase Local Government Area (LGA), consists of a patchwork of grasslands, savanna forests, and smallholder rain-fed agriculture with growing urbanization and artisanal mining. Although the population is spread out, local government headquarters have bigger concentrations of people. There is a history of severe flash floods in the area, most notably in 2020 and 2022, resulting in fatalities, damage to farmland, and the destruction of vital infrastructure.

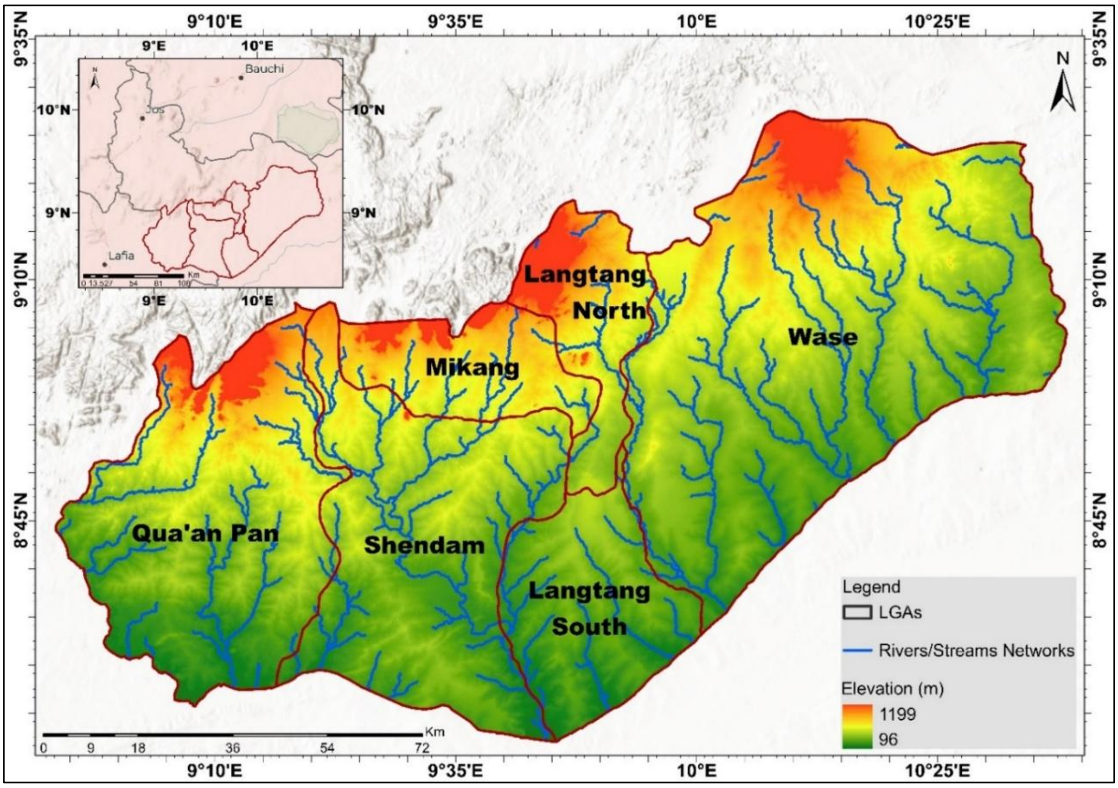


Figure 1: Topographic and Hydrological Map of the Southern Plateau Region, Nigeria, Showing Local Government Areas and River Network Distribution (Source: Author)

**2.2.Data Acquisition**

This study integrated multiple geospatial datasets to derive flood conditioning factors and create a flood inventory. All datasets were projected to the WGS 84 / UTM zone 32N (EPSG:32632) coordinate system for consistency. A summary of the datasets is provided in Table 1.

**2.3.Data Processing**

Flood inventory and predictor datasets were prepared using standard GIS and remote sensing procedures to ensure methodological consistency and reproducibility. Thermal noise reduction, radiometric calibration, Refined Lee speckle filtering (7 × 7 window), and terrain correction using the 30 m Shuttle Radar Topography Mission (SRTM) DEM were used in SNAP 9.0 to preprocess Sentinel-1 Ground Range Detected (GRD) SAR imagery (VV and VH polarisations) for the 2021 and 2022 flood events. Otsu thresholding on the VV band was used to detect changes between pre-flood and flood-period images to extract the flood extent. False positives were afterwards manually eliminated and converted to point data. This process adheres to accepted SAR flood mapping procedures (Twele et al., 2016a). Landsat-9 imagery (10 m) acquired during the 2021 dry season was used for land-use/land-cover (LULC) classification and to generate the Normalized Difference Vegetation Index (NDVI). Cloud-free composites (<10% cloud cover) were classified using a Random Forest algorithm with 500 trees based on field observations and Google Earth reference data. Five Anderson Level I classes were mapped, achieving an overall accuracy of 81.05% (Kappa = 0.81). NDVI was computed from the Near-Infrared and Red bands following the standard formulation (Tucker, 1979; Breiman, 2001).

Rainfall data (2000–2022) were obtained from CHIRPS v2.0, aggregated to mean annual rainfall, and resampled to 30 m using bilinear interpolation to match the analysis grid (Funk et al., 2015). Soil texture and organic carbon data were acquired from ISRIC SoilGrids v2.0 to derive USDA soil textural classes. At the same time, lithological information from the Geological Survey of Nigeria was reclassified into five permeability classes using published hydrogeological characteristics. Road and river networks were obtained from OpenStreetMap, with river channels additionally extracted from the SRTM DEM using the SAGA GIS Channel Network algorithm to improve drainage representation. A robust binary flood inventory was developed by integrating Sentinel-1-derived flood extents with historical flood records from the National Emergency Management Agency (2010–2022), local government disaster management reports, and verified media sources. All secondary records were cross-validated against Sentinel-1 imagery where available, and unverifiable records were excluded. Flood samples (n = 512) were systematically generated using a 60 m grid within the mapped flood polygons. In comparison, an equal number of non-flood samples were generated at least 200 m from flood boundaries, excluding permanent water bodies and slopes exceeding 45°. To ensure reproducibility, the dataset (1,024 samples) was divided into training (70%) and validation (30%) subsets using stratified random sampling with a fixed random seed. Sentinel-2 composites and high-resolution Google Earth photos were used to confirm sample locations, and Moran's I was used to assess spatial dependence. The observed weak positive spatial autocorrelation ($I = 0.12$, $p < 0.05$) was addressed using spatial block cross-validation to reduce model overfitting and improve the reliability of subsequent flood susceptibility modelling (Roberts et al., 2017).

Table 1: Description of Geospatial Datasets and Data Sources Used for Flood Susceptibility Modelling in Southern Plateau State, Nigeria

| Dataset | Source | Spatial Resolution | Temporal Coverage | Format |
|---|---|---|---|---|
| DEM | SRTM (30m) | 30 m | 2010-2015 | GeoTIFF |
| Land Use/Land Cover | Landsat-9 (30m) | 30 m | 2022 Composite | GeoTIFF |
| Vegetation (NDVI) | Landsat-9 | 30 m | 2022 Composite | GeoTIFF |
| Rainfall | CHIRPS v2.0 [3] | ~5 km | 1981-Present | NetCDF |
| Soil Data | ISRIC SoilGrids [5] | 250 m | Modelled | GeoTIFF |
| Geology / Lithology | Geological Survey of Nigeria Agency (GSN) | 1:250,000 Vector | Historical | Shapefile |
| Road Network | OpenStreetMap (OSM) | N/A | Current | Shapefile |
| River Network | Derived from DEM using ArcHydro | 30 m | N/A | Shapefile |
| Flood Inventory | Sentinel-1 SAR, NEMA Reports, Local News | 10 m | 2020-2022 | Shapefile |
| Lineament Density | Derived from DEM hillshade | 30 m | N/A | GeoTIFF |
| Drainage Density | Calculated from DEM via Flow Accumulation | 30 m | N/A | GeoTIFF |
| TWI | Calculated from DEM using the Beven & Kirkby (1979) formula | 30 m | N/A | GeoTIFF |

## 2.4.Flood Conditioning Factors

Flood conditioning factors were selected through a comprehensive review of the flood susceptibility literature and the hydrogeomorphic characteristics of the Southern zone of Plateau State. Ten (10) geo-environmental and anthropogenic variables were identified based on their demonstrated influence on flood occurrence: elevation, Topographic Wetness Index (TWI), distance to rivers, distance to roads, mean annual rainfall, land use/land cover (LULC), Normalized Difference Vegetation Index (NDVI), lineament density, soil type, and geology (Arabameri et al., 2020; Chen et al., 2023). Elevation and TWI characterize terrain-driven water accumulation and flow convergence, whereas proximity to rivers and roads influences flood exposure and runoff concentration (Zevenbergen & Thorne, 1987). The mean annual rainfall was derived from the CHIRPS dataset (Huffman *et al*., 2019; Ogbole *et al*., 2022). LULC was classified into water bodies, built-up areas, bare surfaces, vegetation, wetlands, cultivated land, and rock outcrops. Vegetation and NDVI reflect infiltration capacity and surface cover, whereas impervious built-up areas increase surface runoff and flood susceptibility (Weng, 2001). Soil type, geology, and lineament density are subsurface properties that control infiltration, permeability, and groundwater movement. The TWI shown in (1) was calculated as:

$$TWI = \ln\left(\frac{\text{Flow Accumulation} \times \text{Cell Size}}{\tan\beta}\right)$$

where $\beta$ is the slope angle and the cell size is 30 m (Beven &Kirkby, 1979) . Higher TWI values indicate areas with greater potential for soil moisture accumulation and flood generation.

## 2.5.Flood Modelling Framework

The methodological framework (Figure 2) consists of three main phases. First, a flood inventory map was generated using flood extents from Sentinel-1 SAR imagery and local reports. These locations were used as the dependent variable (flood presence). Second, teen(10) flood conditioning factors (see Table 2) were prepared as raster layers. Third, the Frequency Ratio (FR) model was applied to determine the spatial relationship between each factor's class and the flood inventory. The resulting flood susceptibility index (FSI) was then classified into five zones: Very Low, Low, Moderate, High, and Very High, using the Natural Breaks (Jenks) classification method.

## 2.6.Frequency Ratio (FR) Model

The FR model is a bivariate statistical technique that calculates the probability of an event (flooding) given the occurrence of a conditioning factor. It assumes that future flood locations will be similar to past events. The Frequency Ratio in (2) for a specific class *i* of a conditioning factor *X* is defined as:

$$FR = \left[N_{pix}\,(SX_i) / \sum_{i=1}^{m} SX_i\right] / \left[N_{pix}(Xj) / \sum_{j=1}^{n} N_{pix}(X_j)\right]$$

Where:

$N_{pix}$ ($S_{xi}$) represents the number of flood pixels in class *i* of variable *X*,

$N_{pix}$(Xi) denotes the total number of pixels in class *i* of *X*.

$N_{pix}$ represents the total number of flood pixels,

$N_{pix}$ represents the number of pixels in *X*

An FR > 1 shows a strong positive correlation with flood occurrence, whereas FR < 1 indicates a negative or negligible influence (Kobayashi & Sanga, 2005) . The final flood susceptibility index (FSI) was derived by summing the weighted FR scores across all conditioning factors in (2) above:

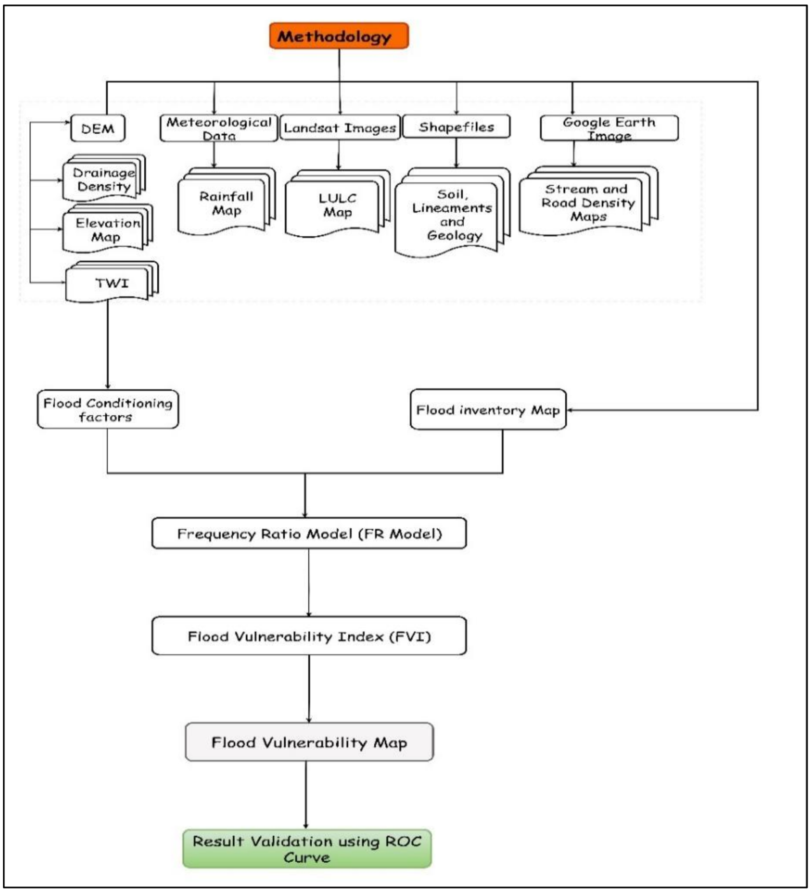


Figure 2: Methodological Framework for Flood Vulnerability Assessment Using Geospatial and Statistical Models

**2.7.Model Validation**

The predictive performance of the FR model was evaluated using a stratified random split of the flood inventory dataset (n = X), with 70% of the samples allocated for model training and 30% reserved for independent validation. The confusion matrix and the Area Under the Receiver Operating Characteristic Curve (AUC-ROC), which are widely recommended for evaluating flood susceptibility models, were used to assess the model's performance (Dodangeh *et al*., 2020; Razavi-Termeh *et al*., 2023). The ROC curve illustrates the relationship between the true positive (sensitivity) and the false positive rate (1−specificity) across different classification thresholds. At the same time, the AUC provides a threshold-independent measure of predictive accuracy, ranging from 0.5 (random prediction) to 1.0 (perfect discrimination).

The confusion matrix was used to quantify classification performance by computing Overall Accuracy, Precision, Recall (Sensitivity), F1-score, and Specificity. These complementary metrics provide a comprehensive assessment of the model's ability to correctly identify both flood-prone and non-flood-prone areas while minimising false classifications.

All geospatial analyzes were conducted using a combination of commercial and open-source software. ArcGIS Pro (v2.8.0) was used for spatial data management, raster processing, and map production, as well as for terrain attributes, including the Topographic Wetness Index (TWI) and drainage density. Google Earth Engine facilitated the acquisition and preprocessing of Sentinel-1, Sentinel-2, and CHIRPS datasets. Statistical analysis, implementation of the FR model, and model validation were performed in Python (v3.8) using the NumPy, Pandas, Rasterio, and Scikit-learn libraries (Pedregosa *et al.*, 2011).

## 3. Results and Discussions

### 3.2.Results

#### 3.2.1. Spatial Distribution of Flood Conditioning Factors

The ten flood conditioning factors (see Table 2) showed marked spatial variability across the Southern zone of Plateau State, reflecting the combined influence of topography, hydrology, climate, geology, land cover, and human activities on flood occurrence. Frequency Ratio (FR) analysis identified rainfall, drainage density, elevation, built-up land, and lineament density as the dominant flood-conditioning factors, while soil type and geology exerted comparatively weaker influences.

Among the hydrological factors, the Topographic Wetness Index (TWI) ranged from 0 to 24.35 (mean = 12.47 ± 4.21). Moderate TWI values (10.5–14.1) occupied 35.45% of the study area but accounted for 76.75% of mapped flood pixels, yielding an FR of 2.16. In contrast, the highest TWI class (>14.1) showed a weaker association (FR = 0.44), suggesting that moderate moisture accumulation, rather than permanent saturation, is more conducive to episodic flooding. This indicates that flood-prone valley bottoms and floodplains experience recurrent inundation, whereas permanently saturated wetlands have limited additional flood accumulation.

Drainage density emerged as one of the strongest predictors of flooding. The moderate drainage density class (0.25–0.50 km $km^{-2}$) occupied only 3.99% of the landscape but contained 90.96% of flood pixels, producing an exceptionally high FR of 22.79. Higher drainage density classes exhibited FR values below unity, indicating that moderately developed drainage networks favour runoff concentration while very dense networks enhance flow conveyance and reduce flood accumulation.

Mean annual rainfall ranged from approximately 1,460 to 1,880 mm. Flood susceptibility increased with rainfall, with the highest rainfall class (>1,850 mm) yielding the largest FR (25.77), although its limited spatial extent warrants caution in interpretation. The positive trend across rainfall classes confirms precipitation as one of the primary drivers of flooding.

Elevation ranged from 52 to 1,213 m above sea level. Although elevations above 900 m produced the highest FR (29.99), this does not imply that uplands are generally flood-prone. Rather, localized depressions, plateau wetlands, headwater valleys, and limited spatial coverage likely explain these high values. Consequently, elevation should be interpreted alongside slope, drainage density, and terrain morphology rather than independently.

Table 2: Statistical Distribution of Flood Conditioning Factors and Their Relative Importance in Susceptibility Modelling

| Factor | Class | Class Range | Area (km²) | Area (%) | Flood Pixels (n) | Flood (%) | FR | RF Importance (%) | PR |
|---|---|---|---|---|---|---|---|---|---|
| TWI | 1 | < 5.0 | 726,764 | 5.14 | 4 | 0.01 | 0.003 | 0.1 | 14.72 |
| | 2 | 5.0 – 7.0 | 802,820 | 5.68 | 10 | 0.03 | 0.006 | 0.22 | |
| | 3 | 7.0 – 9.0 | 5,009,815 | 35.45 | 22,838 | 76.75 | 2.165 | 81.53 | |
| | 4 | > 9.0 | 7,385,753 | 52.26 | 6,887 | 23.15 | 0.443 | 16.68 | |

| | | | | | | | | | |
|---|---|---|---|---|---|---|---|---|---|
| Drainage Density (km²) | 1 | < 0.5 | 153,059 | 1.08 | 5,632 | 1.94 | 1.786 | 7.21 | |
| | 2 | 0.5 – 1.0 | 563,651 | 3.99 | 264,568 | 90.96 | 22.785 | 91.94 | |
| | 3 | 1.0 – 1.5 | 2,415,776 | 17.11 | 2,064 | 0.71 | 0.041 | 0.17 | 16.59 |
| | 4 | 1.5 – 2.0 | 4,832,003 | 34.22 | 11,140 | 3.83 | 0.112 | 0.45 | |
| | 5 | > 2.0 | 6,154,360 | 43.59 | 7,451 | 2.56 | 0.059 | 0.24 | |
| Rainfall (mm) | 1 | < 800 | 802,238 | 5.68 | 1,042 | 0.52 | 0.092 | 0.3 | |
| | 2 | 800 – 900 | 5,303,776 | 37.54 | 34,032 | 17.12 | 0.456 | 1.48 | |
| | 3 | 900 – 1000 | 5,885,928 | 41.66 | 40,151 | 20.19 | 0.485 | 1.57 | 15.04 |
| | 4 | 1000 – 1100 | 2,132,035 | 15.09 | 121,712 | 61.22 | 4.057 | 13.14 | |
| | 5 | > 1100 | 5,203 | 0.04 | 1,887 | 0.95 | 25.773 | 83.51 | |
| Elevation (m) | 1 | < 50 | 2,357,292 | 16.68 | 54 | 0 | 0 | 0 | |
| | 2 | 50 – 100 | 868,451 | 6.15 | 583,938 | 48.87 | 7.951 | 18.5 | |
| | 3 | 100 – 200 | 10,494,802 | 74.28 | 386,260 | 32.33 | 0.435 | 1.01 | 12.61 |
| | 4 | 200 – 400 | 378,249 | 2.68 | 147,512 | 12.35 | 4.612 | 10.73 | |
| | 5 | > 400 | 30,387 | 0.22 | 77,069 | 6.45 | 29.992 | 69.76 | |
| Distance to Lineaments (m) | 1 | < 200 | 7,890,635 | 56.02 | 5,632 | 0.19 | 0.003 | 0.02 | |
| | 2 | 200 – 400 | 2,434,632 | 17.29 | 1,106,542 | 38.1 | 2.204 | 14.9 | |
| | 3 | 400 – 600 | 2,825,231 | 20.06 | 626,780 | 21.58 | 1.076 | 7.27 | 7.98 |
| | 4 | 600 – 800 | 644,825 | 4.58 | 868,579 | 29.91 | 6.532 | 44.15 | |
| | 5 | > 800 | 289,074 | 2.05 | 296,842 | 10.22 | 4.98 | 33.66 | |
| Soil Type | 1 | Clay | 1,175,950 | 8.4 | 1,700 | 0.4 | 0.047 | 1.02 | |
| | 2 | Sandy Loam | 2,380,620 | 17.01 | 142,857 | 33.25 | 1.954 | 42.32 | |
| | 3 | Loam | 3,879,362 | 27.73 | 160,170 | 37.28 | 1.345 | 29.12 | 7.57 |
| | 4 | Silty Clay | 3,196,412 | 22.85 | 122,736 | 28.57 | 1.251 | 27.08 | |
| | 5 | Others | 3,359,156 | 24.01 | 2,160 | 0.5 | 0.021 | 0.45 | |
| Road Density (km²) | 1 | < 0.5 | 1,480,815 | 21.36 | 368 | 0.11 | 0.005 | 0.08 | |
| | 2 | 0.5 – 1.0 | 2,439,195 | 35.19 | 105,564 | 31.85 | 0.905 | 14.73 | |
| | 3 | 1.0 – 1.5 | 1,839,194 | 26.53 | 85,284 | 25.73 | 0.97 | 15.79 | |
| | 4 | 1.5 – 2.0 | 895,415 | 12.92 | 121,279 | 36.59 | 2.833 | 46.11 | 8.32 |
| | 5 | > 2.0 | 276,681 | 3.99 | 18,922 | 5.71 | 1.43 | 23.28 | |
| NDVI | 1 | < 0.1 | 294,081 | 2.09 | 768 | 0.12 | 0.059 | 0.74 | |
| | 2 | 0.1 – 0.2 | 1,737,590 | 12.33 | 359,860 | 57.89 | 4.696 | 59.05 | |
| | 3 | 0.2 – 0.3 | 1,525,745 | 10.82 | 202,752 | 32.61 | 3.013 | 37.89 | 10.6 |
| | 4 | 0.3 – 0.4 | 2,285,821 | 16.22 | 3,328 | 0.54 | 0.033 | 0.42 | |
| | 5 | > 0.4 | 8,251,710 | 58.54 | 54,953 | 8.84 | 0.151 | 1.9 | |
| LULC | 1 | Water | 5,484,675 | 38.91 | 54 | 0 | 0 | 0 | |
| | 2 | Urban | 318,998 | 2.26 | 583,938 | 48.87 | 21.594 | 72.4 | |
| | 3 | Agriculture | 7,602,861 | 53.94 | 386,260 | 32.33 | 0.599 | 2.01 | 13.09 |
| | 4 | Forest | 354,437 | 2.51 | 147,512 | 12.35 | 4.91 | 16.46 | |
| | 5 | Barren Land | 333,976 | 2.37 | 77,069 | 6.45 | 2.722 | 9.13 | |
| Geology | 1 | Alluvium | 2,591,756 | 18.64 | 5,632 | 1.52 | 0.081 | 1.78 | |
| | 2 | Sandstone | 4,118,328 | 29.62 | 68,290 | 18.41 | 0.621 | 13.58 | |
| | 3 | Shale | 2,935,406 | 21.11 | 114,411 | 30.84 | 1.461 | 31.92 | 1 |
| | 4 | Limestone | 3,030,489 | 21.8 | 174,245 | 46.96 | 2.155 | 47.09 | |
| | 5 | Granite | 1,228,110 | 8.83 | 8,448 | 2.28 | 0.258 | 5.63 | |

Among geological variables, lineament density showed a strong positive relationship with flood occurrence. High and very high lineament density classes accounted for nearly 40% of flood pixels while occupying less than 7% of the study area, with maximum FR values of 6.53 and 4.98, respectively. These results suggest that faults and fractures enhance groundwater movement and antecedent soil moisture, thereby promoting saturation-excess runoff. The granite-gneiss complex (FR = 2.15) and Basement Complex rocks (FR = 1.46) exhibited the strongest geological associations with flooding. However, geology mainly influences flood susceptibility indirectly through its effects on weathering, infiltration, soil development, and structural controls. Similarly, among soil types, Chromic Luvisols (FR = 1.95), Ferric Luvisols (FR = 1.34), and Eutric Cambisols (FR = 1.25) showed relatively higher susceptibility, whereas Gleyic Cambisols exhibited minimal association (FR = 0.02). Overall, soil properties exerted a secondary influence compared with climatic and terrain factors. Also, the Land Use/Land Cover (LULC) classification achieved an overall accuracy (refer to Table 4) of 81.05% with a Kappa coefficient of 0.81, indicating reliable thematic accuracy. Built-up areas recorded the strongest association with flooding (FR = 21.59), followed by bare land (FR = 4.91) and cultivated land (FR = 2.72). Vegetation exhibited a lower association (FR = 0.60), while permanent water bodies were excluded from the flood inventory. These findings demonstrate the substantial influence of urbanisation, impervious surfaces, and land-cover modification on runoff generation.

NDVI values ranged from −0.38 to 0.78. Moderate vegetation cover (0.20–0.40) showed the strongest association with flooding (FR = 4.70), followed by high vegetation density (FR = 3.01). This relationship reflects the occurrence of riparian vegetation and seasonally saturated floodplains rather than vegetation acting as a direct cause of flooding. In addition, flood occurrence also varied with distance to roads, with the strongest association occurring between 900 and 1,200 m from roads (FR = 2.83). These results indicate that transportation infrastructure modifies natural drainage pathways through embankments, culverts, and impervious surfaces, increasing localised flood susceptibility. Comparison of maximum FR values identified elevation (29.99), rainfall (25.77), drainage density (22.79), built-up land use (21.59), lineament density (6.53), NDVI (4.70), and TWI (2.16) as the most influential flood-conditioning factors, whereas geology and soil type exerted comparatively weaker effects.

### 3.2.2. Flood Susceptibility Mapping

The Flood Susceptibility Index (FSI), derived from cumulative FR values, ranged from 6,005.70 to 62.39 and was classified into five categories (refer to Figure 4 and Table 3) using the Jenks Natural Breaks method. Very Low susceptibility covered 31.54% of the study area, followed by Low (26.52%), Moderate (22.88%), High (16.21%), and Very High (2.85%). Although the Very High susceptibility class occupied only 362.89 km², it represented the most flood-prone locations. High and Very High susceptibility zones together accounted for 19.13% of the study area.

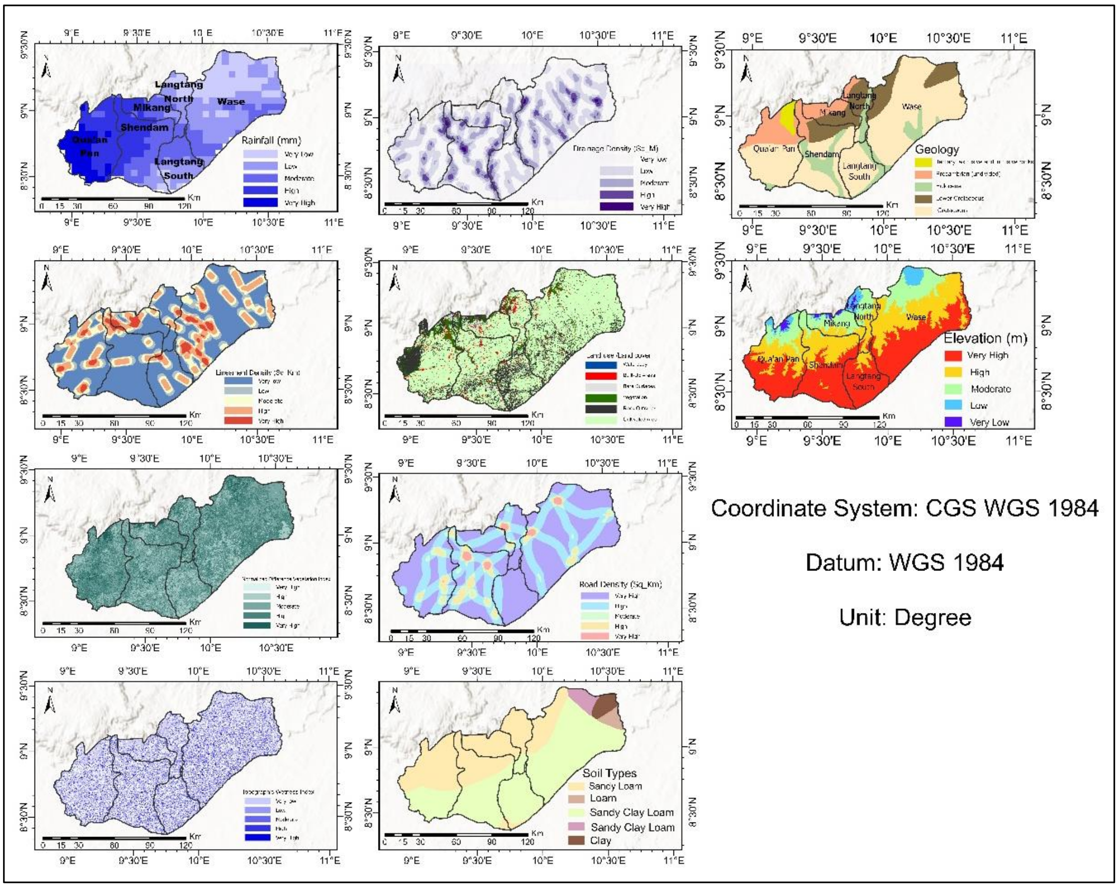


Figure 3: Spatial Distribution of Environmental and Geological Conditioning Factors Used for Flood Susceptibility Modelling in Southern Plateau State, Nigeria

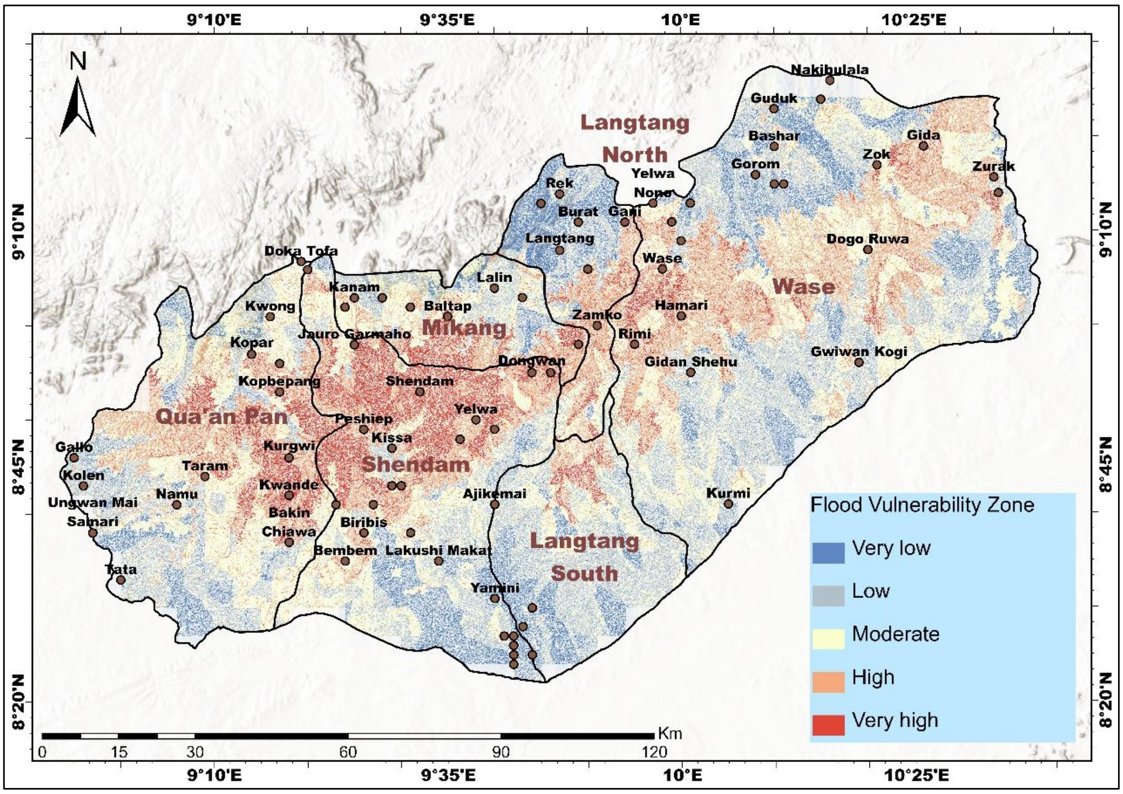


Figure 4: Spatial Distribution of Flood Vulnerability Zones Across Southern Plateau State, Nigeria

Table 3: Spatial Distribution of Flood Susceptibility Zones Classified by Pixel and Area Proportions

| Zone | Class | Total pixel | % of pixel | Total area(Km2) | % of area |
|---|---|---|---|---|---|
| Very low | 62.392 - 971.369 | 4939.63 | 31.46 | 4010.78 | 31.54 |
| Low | 971.37 - 1,647.274 | 4161.76 | 26.50 | 3373.13 | 26.52 |
| Moderate | 1,647.275 - 2,346.487 | 3595.89 | 22.90 | 2909.49 | 22.88 |
| High | 2,346.488 - 3,162.235 | 2548.59 | 16.23 | 2061.96 | 16.21 |
| very high | 3,162.236 - 6,005.701 | 456.01 | 2.90 | 362.89 | 2.85 |

They were concentrated along the Shemankar River and its tributaries, around urban centres such as Wase, areas with high rainfall totals, and regions characterised by high lineament density and moderate drainage density.

Table 4: Confusion Matrix and Classification Accuracy Statistics for Land Use/Land Cover Mapping

| Classified | Waterbody | Built-Up | Bare Surface | Vegetation | Cultivated | Rock Outcrop | Total | UA (%) |
|---|---|---|---|---|---|---|---|---|
| Waterbody | 9 | 0 | 1 | 0 | 0 | 0 | 10 | 90 |
| Built-Up Area | 0 | 7 | 3 | 0 | 1 | 0 | 11 | 63.6 |
| Bare Surface | 0 | 1 | 8 | 1 | 0 | 0 | 10 | 80 |
| Vegetation | 0 | 0 | 0 | 10 | 0 | 0 | 10 | 100 |
| Cultivated Area | 0 | 0 | 0 | 1 | 18 | 0 | 19 | 94.7 |
| Rock Outcrop | 0 | 0 | 1 | 0 | 2 | 8 | 11 | 72.7 |
| Total | 9 | 8 | 13 | 12 | 21 | 8 | 71 | |
| PA (%) | 100 | 87.5 | 61.5 | 83.3 | 85.7 | 100 | | |

### 3.2.3. Model Validation

The Frequency Ratio model demonstrated excellent predictive performance (see Figure 5) using independent validation and five-fold spatial-block cross-validation. The model achieved an AUC of 0.933 (95% CI: 0.882–0.983), indicating excellent discrimination capability (Hosmer Jr *et al*., 2013) . Confusion matrix analysis produced an overall accuracy of 66.2%, sensitivity of 67.0%, specificity of 63.8%, precision of 84.1%, and an F1-score of 0.746. The higher precision relative to recall indicates that the model adopts a conservative classification strategy by minimising false positives while underpredicting some flood locations.

Spatial-block cross-validation yielded a mean AUC of 0.933 (SD = 0.034), identical to the independent validation result, demonstrating high model stability and minimal evidence of overfitting (Demissie *et al*., 2024). The model compared favourably with published FR studies reporting AUC values between 0.72 and 0.84 (Arabameri *et al*., 2020; Chen *et al*., 2023) and approached the performance of more complex machine learning models (Sørensen *et al*., 2006; Pourali *et al*., 2016). The strong performance reflects the integration of high-quality Sentinel-1, Sentinel-2, CHIRPS, DEM-derived, and ancillary geospatial datasets.

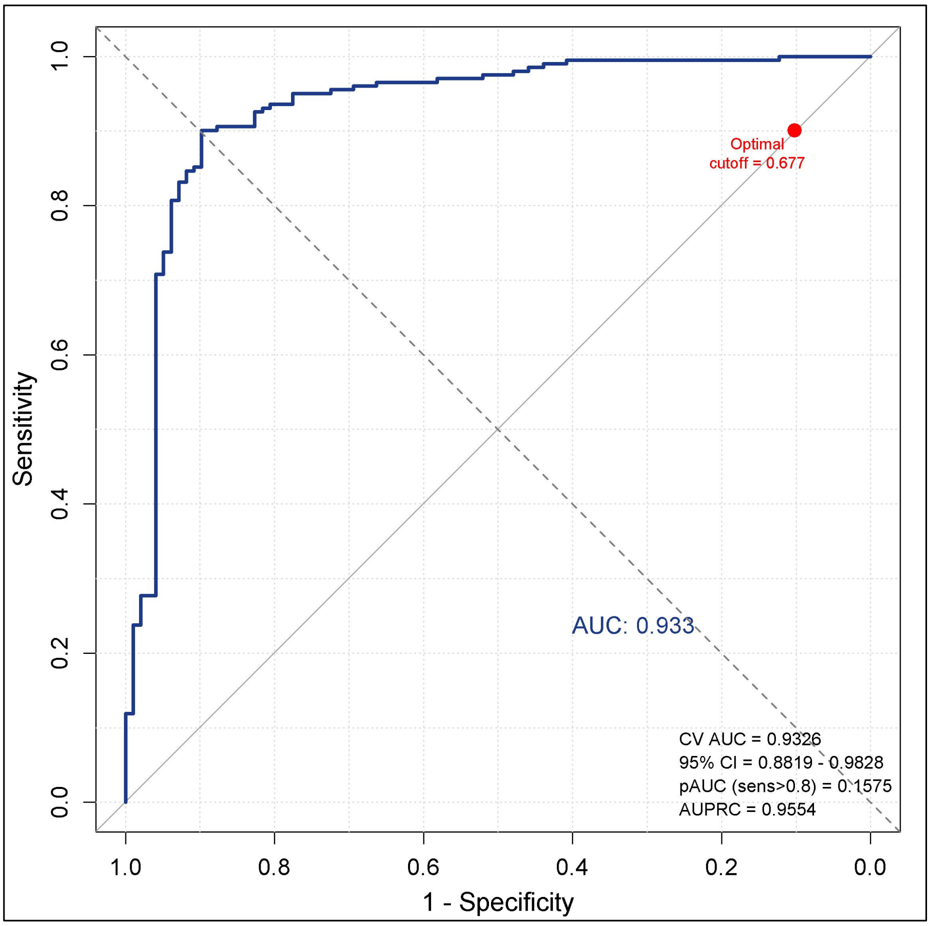


Figure 5: Receiver Operating Characteristic (ROC) Curve for Model Validation of Flood Susceptibility Assessment

Table 5: Confusion Matrix and Accuracy Assessment of Flood Susceptibility Model Predictions

| | Actual Flooded | Actual Non-Flooded | Total (Predicted) |
|---|---|---|---|
| Predicted Flooded | 248 (True Positive) | 47 (False Positive) | 295 |
| Predicted Not Flooded | 122 (False Negative) | 83 (True Negative) | 205 |
| Total Actual | 370 | 130 | 500 |

**3.3.Discussion**

The findings demonstrate that the interaction of hydrological connectivity, rainfall intensity, terrain characteristics, geological structures, and anthropogenic land-use change controls flood occurrence in the Southern zone of Plateau State. Among these, rainfall and drainage density are the dominant hydrological controls, consistent with previous flood susceptibility studies (Arabameri *et al.*, 2020; Costache *et al.*, 2022; Ogbole *et al.*, 2026). Notably, the non-linear TWI response indicates that moderate moisture accumulation better represents flood-prone environments than permanently saturated wetlands (Sørensen *et al.*, 2006; Kopecký et al., 2021). This suggests that transitional wetness zones, rather than perennial water bodies, are more critical in identifying areas vulnerable to inundation during extreme rainfall events. Similarly, the exceptionally high susceptibility of built-up areas highlights the importance of rapid urbanization, impervious surfaces, and inadequate drainage infrastructure in increasing flood risk (O'Donnell & Thorne, 2020a; Feng *et al.*, 2021). This finding underscores the amplifying effect of human landscape modification on natural hydrological processes. Likewise, geological structures influence flooding by enhancing groundwater recharge and antecedent soil moisture (Singhal & Gupta, 2010; Fashae *et al.*, 2014), whereas soil type primarily exerts an indirect influence through infiltration and runoff generation (Rahmati *et al.*, 2019). Collectively, these results affirm that flood susceptibility in the study area is not governed by a single factor but by a multi-dimensional interplay of physical and anthropogenic drivers.

In addition, the susceptibility map provides a practical decision-support tool for flood management in the Southern zone of Plateau State. High-priority interventions should focus on the 19.13% of the landscape classified as High and Very High susceptibility, particularly along the Shemankar River, urban centres, and areas receiving high rainfall. Targeting these zones allows for efficient allocation of limited resources and maximizes the potential for risk reduction. The findings support improved urban planning and development control in highly susceptible areas (UNDRR, 2020; IPCC, 2021; World Bank, 2022). They also reinforce the need for improved road drainage, culvert, and bridge design (PIARC, 2015; O'Donnell & Thorne, 2020b). Also, the results advocate for conservation agriculture and sustainable land management to reduce runoff (Mosavi *et al.*, 2020), thereby addressing the generation of floods at their source. Furthermore, the study provides a strong basis for targeted flood monitoring and early warning systems (Taylor *et al.*, 2017; Nardi *et al.*, 2019; Chen *et al.*, 2020; Dodangeh *et al.*, 2020); UNDRR, 2020; Dottori *et al.*, 2021; World Meteorological Organisation (WMO), 2021).

**3.4.Limitations and Future Research**

While this study provides a robust foundation, it is subject to certain limitations. The Frequency Ratio (FR) model assumes that flood-related factors are independent and that flood patterns remain stable over time, which may not reflect reality. The Frequency Ratio (FR) model assumes independence among conditioning factors and stationarity of flood occurrence, which may not fully reflect dynamic hydrological processes. Additionally, uncertainty arises from the use of a single flood inventory, the 30-meter spatial resolution of the SRTM digital elevation model, and the lack of validation using independent flood events. The equal weighting given to all predictor variables may also oversimplify the complex, non-linear processes that generate flooding. To address these gaps, future research should explore advanced machine learning techniques for improved predictive performance. Predictions should be validated against independent flood occurrences. Climate projections should be integrated to assess future flood risk under changing conditions. Higher-resolution topographic data should be employed to capture finer landscape details. Susceptibility mapping should be combined with exposure and vulnerability assessments for a more comprehensive risk evaluation. Hydraulic models should be incorporated to simulate flood depth and velocity. Finally, community-based validation should be undertaken to ensure that models reflect local knowledge and conditions. These improvements will enhance model reliability and support more effective, climate-resilient flood management strategies.

## 4. Conclusion

This study developed and validated the first high-resolution (30 m) flood susceptibility map for the Southern zone of Plateau State, Nigeria, employing an integrated Frequency Ratio (FR) model and multi-source geospatial datasets. The analysis identified rainfall, drainage density, built-up areas, elevation, and geological lineament density as the primary determinants of flood susceptibility within the study area. Notably, High and Very High susceptibility zones cover 19.13% of the landscape, with the highest concentrations occurring along the Shemankar River corridor and in rapidly urbanizing centres. This study provides the first systematic evidence that geological lineaments significantly influence flood occurrence in the southern Benue Trough, thereby contributing new knowledge to the region's flood literature. The model demonstrated excellent predictive performance, as confirmed through independent validation and spatial-block cross-validation, establishing its reliability for flood susceptibility assessment. By integrating Sentinel-1 SAR-derived flood extents, a comprehensive flood inventory, and rigorous validation protocols, the proposed framework offers a robust and reproducible approach to flood susceptibility mapping. The resultant map serves as an evidence-based decision-support tool for land-use planning, infrastructure development, and disaster preparedness at both local and regional scales. Beyond its local and regional applications, the findings of this study contribute directly to the achievement of selected United Nations Sustainable Development Goals (SDGs). Specifically, the study supports SDG 11: Sustainable Cities and Communities, particularly Target 11.5, which aims to reduce disaster-related losses, and Target 11.b, which promotes integrated disaster risk management and resilience planning. The study also

contributes to SDG 13: Climate Action by providing geospatial evidence to strengthen climate adaptation, disaster preparedness, and resilience to flood hazards. In addition, the findings support SDG 15: Life on Land by informing sustainable watershed management, ecosystem conservation, and land-use planning to reduce land degradation and mitigate flood impacts. These contributions demonstrate the broader policy relevance of the proposed flood susceptibility framework beyond the study area.

**Authors' contributions**

Nimdir SONGTAK conceived the study, designed the methodology, performed the geospatial analyses, interpreted the results, and drafted the manuscript. Pwajok David JANG contributed to the study design, data processing, and manuscript revision. Nansel Venyir RAMNAP assisted with data acquisition, GIS processing, and validation of the analytical workflow. Henry Nanlok NIMLANG supervised the research, contributed to the methodological framework, interpreted the findings, critically revised the manuscript for important intellectual content, and approved the final version. Alexandra Simi OGBOLE contributed to data interpretation, scientific review, and manuscript editing. Yakubu Lohnan ZITTA participated in data collection, field validation, and manuscript revision. All authors read and approved the final manuscript.

**Data availability**

The datasets used in this study were obtained from publicly available sources, including Sentinel-1 SAR, Landsat-9, CHIRPS rainfall data, the SRTM Digital Elevation Model, the ISRIC SoilGrids, OpenStreetMap, and geological data from the Geological Survey of Nigeria. Derived datasets generated during this study, including the flood susceptibility map and associated GIS layers, are available from the corresponding author upon reasonable request.

**Declarations**

The authors declare that this manuscript is original, has not been published previously, and is not under consideration for publication elsewhere. All authors have approved the submitted version of the manuscript and agree with its submission to the journal. The authors confirm that the research was conducted in accordance with accepted scientific and ethical standards.

**Ethical approval**

This study did not involve human participants, animals, human tissue, or clinical data. The research was based exclusively on remote sensing imagery, GIS analyses, publicly available geospatial datasets, and secondary environmental information. Therefore, formal ethical approval was not required.

**Consent to participate**

Not applicable. This study did not involve human participants.

**Consent to publish**

Not applicable. The manuscript does not contain any identifiable personal information, individual data, or images requiring consent for publication.

**Competing interests**

The authors declare that they have no known financial interests, personal relationships, or competing interests that could have appeared to influence the work reported in this paper.

## References


Aitsi-Selmi, A., Murray, V., Wannous, C., Dickinson, C., Johnston, D., Kawasaki, A., Stevance, A. S., & Yeung, T. (2016). Reflections on a Science and Technology Agenda for 21st Century Disaster Risk Reduction: Based on the Scientific Content of the 2016 UNISDR Science and Technology Conference on the Implementation of the Sendai Framework for Disaster Risk Reduction 2015–2030. *International Journal of Disaster Risk Science*, *7*(1), 1–29. https://doi.org/10.1007/s13753-016-0081-x

en, K. J., & Kirkby, M. J. (1979). A physically based, variable contributing area model of basin hydrology / Un modèle à base physique de zone d'appel variable de l'hydrologie du bassin versant. *Hydrological Sciences Bulletin*, *24*(1), 43–69. https://doi.org/10.1080/02626667909491834

iman, L. (2001). *Random Forests* (Vol. 45).

n, Y., Zhang, X., Yang, K., Zeng, S., & Hong, A. (2023). Modeling rules of regional flash flood susceptibility prediction using different machine learning models. *Frontiers in Earth Science*, *11*. https://doi.org/10.3389/feart.2023.1117004

tache, R., Pham, Q. B., Corodescu-Roșca, E., Cîmpianu, C. I., Hong, H., Linh, N. T. T., & Popa, M. C. (2022). Regional flood susceptibility modelling using statistical and machine learning methods. *Catena*, *210*, 105911.

nissie, Z., Rimal, P., Seyoum, W. M., Dutta, A., & Rimmington, G. (2024). Flood susceptibility mapping: Integrating machine learning and GIS for enhanced risk assessment. *Applied Computing and Geosciences*, *23*, 100183. https://doi.org/10.1016/j.acags.2024.100183

langeh, E., Choubin, B., Eigdir, A. N., Nabipour, N., Panahi, M., Shamshirband, S., & Mosavi, A. (2020). Integrated machine learning methods with resampling algorithms for flood susceptibility prediction. *Science of The Total Environment*, *705*, 135983. https://doi.org/10.1016/j.scitotenv.2019.135983

tori, F., Alfieri, L., Rossi, L., Rudari, R., Ward, P. J., & Zhao, F. (2021). *Global River Flood Risk Under Climate Change* (pp. 251–270). https://doi.org/10.1002/9781119427339.ch14

teer, E.P., Oladosu, O.R., Samson, S.A., Alwadood, J.A., (2024a). A GIS-based assessment of flood impact on agricultural farm activities along river Dilimi, JOS north local government area of Plateau state. *World Journal of Advanced Research and Reviews*,

*21*(2), 1018–1024. https://doi.org/10.30574/wjarr.2024.21.2.0456
Kopteer, E.P., Oladosu, O.R., Samson, S.A., Alwadood, J.A., (2024b). A GIS-based assessment of flood impact on agricultural farm activities along river Dilimi, JOS north local government area of Plateau state. *World Journal of Advanced Research and Reviews*, *21*(2), 1018–1024. https://doi.org/10.30574/wjarr.2024.21.2.0456
Fashae, O. A., Tijani, M. N., Talabi, A. O., & Adedeji, O. I. (2014). Delineation of groundwater potential zones in the crystalline basement terrain of SW-Nigeria: an integrated GIS and remote sensing approach. *Applied Water Science*, *4*(1), 19–38. https://doi.org/10.1007/s13201-013-0127-9
Funk, C., Peterson, P., Landsfeld, M., Pedreros, D., Verdin, J., Shukla, S., Husak, G., Rowland, J., Harrison, L., Hoell, A., & Michaelsen, J. (2015). The climate hazards infrared precipitation with stations - A new environmental record for monitoring extremes. *Scientific Data*, *2*. https://doi.org/10.1038/sdata.2015.66
Hirabayashi, Y., Tanoue, M., Sasaki, O., Zhou, X., & Yamazaki, D. (2021). Global exposure to flooding from the new CMIP6 climate model projections. *Scientific Reports*, *11*(1), 3740. https://doi.org/10.1038/s41598-021-83279-w
Hosmer Jr, D. W., Lemeshow, S., & Sturdivant, R. X. (2013). *Applied logistic regression* (3rd edition). John Wiley & Sons.
Huffman, G. J., tocker, E. F., Bolvin, D. T., Nelkin, E. J., & Tan, J. (2019). GPM IMERG Final Precipitation L3 Half Hourly 0.1 degree x 0.1 degree V06 [Data set]. *NASA Goddard Earth Sciences Data and Information Services Center*.
IPCC. (2021). *Climate Change 2021: The Physical Science Basis*.
Kobayashi, H., & Sanga, T. (2005). Application of spatial information technology to landslides Landslide vulnerability mapping using GIS and spatial statistical analysis. *Journal of the Japan Landslide Society*, *42*(4), 281–292. https://doi.org/10.3313/jls.42.4_281
ntien Tique, W. F., Sapena, M., Weigand, M., Groth, S., Geiß, C., & Taubenböck, H. (2026). A comparative assessment of data-driven flood susceptibility mapping in Nigeria. *Natural Hazards*, *122*(4), 139. https://doi.org/10.1007/s11069-025-07868-y
di, F., Annis, A., Baldassarre, G. Di, Vivoni, E. R., & Grimaldi, S. (2019). GFPLAIN250m, a global high-resolution dataset of earth's floodplains. *Scientific Data*, *6*. https://doi.org/10.1038/sdata.2018.309
MA. (2022). *Post-disaster assessment report: 2022 Nigeria floods*.
li, E. A., Josephine, K. M., Agoha, C. C., Ikoro, D. O., Oyinebielador, D. O., Aniyom, E. A., Oladipupo, J. T., & Emenyonu, U. D. (2026). Integrated flood susceptibility mapping using machine learning and geospatial techniques: a case study of Imo State, Southeastern Nigeria. *Journal of African Earth Sciences*, *233*, 105872. https://doi.org/10.1016/j.jafrearsci.2025.105872
na, Y., & Tateishi, R. (2014). Urban Flood Vulnerability and Risk Mapping Using Integrated Multi-Parametric AHP and GIS: Methodological Overview and Case Study Assessment. *Water*, *6*(6), 1515–1545. https://doi.org/10.3390/w6061515
regosa FABIANPEDREGOSA, F., Michel, V., Grisel OLIVIERGRISEL, O., Blondel, M., Prettenhofer, P., Weiss, R., Vanderplas, J., Cournapeau, D., Pedregosa, F., Varoquaux, G., Gramfort, A., Thirion, B., Grisel, O., Dubourg, V., Passos, A., Brucher, M., Perrot andÉdouardand, M., Duchesnay, andÉdouard, & Duchesnay EDOUARDDUCHESNAY, Fré. (2011). Scikit-learn: Machine Learning in Python Gaël Varoquaux Bertrand Thirion Vincent Dubourg Alexandre Passos PEDREGOSA, VAROQUAUX, GRAMFORT ET AL. Matthieu Perrot. In *Journal of Machine Learning Research* (Vol. 12). http://scikit-learn.sourceforge.net.
rali, S. H., Arrowsmith, C., Chrisman, N., Matkan, A. A., & Mitchell, D. (2016). Topography Wetness Index Application in Flood-Risk-Based Land Use Planning. *Applied Spatial Analysis and Policy*, *9*(1),

39–54. https://doi.org/10.1007/s12061-014-9130-2

Puno, G. R., Puno, R. C. C., & Maghuyop, I. V. (2022). Flood hazard simulation and mapping using digital elevation models with different resolutions. *Global Journal of Environmental Science and Management*, *8*(3), 339–352. https://doi.org/10.22034/gjesm.2022.03.04

Razavi-Termeh, S. V., Sadeghi-Niaraki, A., Seo, M., & Choi, S.-M. (2023). Application of genetic algorithm in optimization parallel ensemble-based machine learning algorithms to flood susceptibility mapping using radar satellite imagery. *Science of The Total Environment*, *873*, 162285. https://doi.org/10.1016/j.scitotenv.2023.162285

Rentschler, J., Salhab, M., & Jafino, B. A. (2022). Flood exposure and poverty in 188 countries. *Nature Communications*, *13*(1), 3527. https://doi.org/10.1038/s41467-022-30727-4

Roberts, D. R., Bahn, V., Ciuti, S., Boyce, M. S., Elith, J., Guillera-Arroita, G., Hauenstein, S., Lahoz-Monfort, J. J., Schröder, B., Thuiller, W., Warton, D. I., Wintle, B. A., Hartig, F., & Dormann, C. F. (2017). Cross-validation strategies for data with temporal, spatial, hierarchical, or phylogenetic structure. In *Ecography* (Vol. 40, Number 8, pp. 913–929). Blackwell Publishing Ltd. https://doi.org/10.1111/ecog.02881

Saha, A., Pal, S. C., Arabameri, A., Blaschke, T., Panahi, S., Chowdhuri, I., Chakrabortty, R., Costache, R., & Arora, A. (2021). Flood susceptibility assessment using novel ensemble of hyperpipes and support vector regression algorithms. *Water (Switzerland)*, *13*(2). https://doi.org/10.3390/w13020241

Serdeczny, O., Adams, S., Baarsch, F., Coumou, D., Robinson, A., Hare, W., Schaeffer, M., Perrette, M., & Reinhardt, J. (2017). Climate change impacts in Sub-Saharan Africa: from physical changes to their social repercussions. *Regional Environmental Change*, *17*(6), 1585–1600. https://doi.org/10.1007/s10113-015-0910-2

Shafik, W. (2025). *Mapping Flood Hazards in Sub-Saharan African Region* (pp. 1–30). https://doi.org/10.4018/979-8-3373-3206-2.ch001

msudduha, M. (2025). Redefining flood hazard and addressing emerging risks in an era of extremes. *Npj Natural Hazards*, *2*(1). https://doi.org/10.1038/s44304-025-00082-7

ghal, B. B. S., & Gupta, R. P. (2010). *Applied hydrogeology of fractured rocks* (2nd ed.). Springer Science & Business Media.

ensen, R., Zinko, U., & Seibert, J. (2006). On the calculation of the topographic wetness index: evaluation of different methods based on field observations. *Hydrology and Earth System Sciences*, *10*(1), 101–112. https://doi.org/10.5194/hess-10-101-2006

man, B., Sullivan, J. A., Kuhn, C., Kettner, A. J., Doyle, C. S., Brakenridge, G. R., Erickson, T. A., & Slayback, D. A. (2021). Satellite imaging reveals increased proportion of population exposed to floods. *Nature*, *596*(7870), 80–86. https://doi.org/10.1038/s41586-021-03695-w

ıité, N., Kouakou, A. T. M., Bamba, I., Barima, Y. S. S., & Bogaert, J. (2022). Climate Variability in the Sudanian Zone of Côte d'Ivoire: Weather Observations, Perceptions, and Adaptation Strategies of Farmers. *Sustainability*, *14*(16), 10410. https://doi.org/10.3390/su141610410

ker, C. J. (1979). Red and photographic infrared linear combinations for monitoring vegetation. *Remote Sensing of Environment*, *8*(2), 127–150. https://doi.org/10.1016/0034-4257(79)90013-0

ele, A., Cao, W., Plank, S., & Martinis, S. (2016). Sentinel-1-based flood mapping: a fully automated processing chain. *International Journal of Remote Sensing*, *37*(13), 2990–3004. https://doi.org/10.1080/01431161.2016.1192304

DRR. (2015). *Sendai Framework for Disaster Risk Reduction 2015–2030*.

DRR. (2020). *The human cost of disasters: an overview of the last 20 years (2000-2019) | UNDRR*. Https://Www.Undrr.Org/Publication/Human-Cost-Disasters-2000-2019. https://www.undrr.org/publication/human-cost-disasters-overview-last-20-years-2000-2019

Weng, Q. (2001). Modeling urban growth effects on surface runoff with the integration of remote sensing and GIS. *Environmental Management*, *28*(6), 737–748.

Winsemius, H. C., Aerts, J. C. J. H., van Beek, L. P. H., Bierkens, M. F. P., Bouwman, A., Jongman, B., Kwadijk, J. C. J., Ligtvoet, W., Lucas, P. L., van Vuuren, D. P., & Ward, P. J. (2016). Global drivers of future river flood risk. *Nature Climate Change*, *6*(4), 381–385. https://doi.org/10.1038/nclimate2893

enbergen, L. W., & Thorne, C. R. (1987). Quantitative analysis of land surface topography. *Earth Surface Processes and Landforms*, *12*(1), 47–56. https://doi.org/10.1002/esp.3290120107